Zero-Shot State Identification of Industrial Gas–Liquid Two-Phase Flow via Supervised Deep Slow and Steady Feature Analysis

Linghan Li, Xinyi Han, Feng Dong, *Senior Member, IEEE*, and Shumei Zhang, *Member, IEEE*

***Abstract*—Gas–liquid two-phase flow is a complex dynamic and nonlinear process that is widely encountered in many process industries. Accurate flow state identification is crucial for ensuring operation safety and economic benefits. However, obtaining training samples for certain flow states can be difficult due to safety requirements and high costs. Therefore, a zero-shot learning (ZSL) based flow state identification strategy is proposed from the perspective of attribute description and attribute transfer, in which the common attribute space is constructed by the semantic description of flow state categories. The attribute-relevant features are extracted by the proposed supervised deep slow and steady feature analysis (SD-S^{2}FA) under the supervision of attributes. In SD-S^{2}FA, an extended Siamese network is designed to extract slow and steady features (S^{2}Fs), in which three 1D convolutional neural networks (1D-CNN) represent the nonlinear feature embedding function, and the Siamese architecture can capture the long-term temporal coherence. Since the state attributes are shared by all the flow states, the identification for unseen flow states can be realized by attribute prediction and attribute transfer. The effectiveness and superiority of the proposed method is demonstrated through the gas–liquid two-phase flow experiment.**

***Index Terms*—Gas–liquid two-phase flow, state identification, supervised deep slow and steady feature (S^{2}FA) analysis (SD-S^{2}FA), zero-shot learning (ZSL).**

I. Introduction

GAS–LIQUID two-phase flow is a complex dynamic and nonlinear process, which commonly exists in important industrial fields, such as petroleum and chemical engineering [1]. Owing to the influence of various flow conditions and parameters, the two-phase flow process exhibits a wide range of flow states, including typical states and transition states. Each flow state has a distinct impact on production and transportation, and certain hazardous states, such as slug flow, have the potential to cause severe damage to industrial facilities. Therefore, accurate identification of flow states is essential for ensuring operational safety and economic benefits. To obtain flow process data and monitor flow processes, a variety of sensors based on electric [2], [3], ultrasonic [4], radiation [5], and optics [6] have been developed. Due to the high complexity of multiphase flow process mechanisms, data-driven methods have garnered immense attention in flow state identification and flow process monitoring [7].

In recent data-driven studies for industrial processes, multivariate statistical methods cored with principle component analysis (PCA) [8] and partial least square (PLS) [9] have drawn widespread interest due to their excellent abilities in feature extraction and dimension reduction. To distill temporal information for dynamic processes, slow feature analysis (SFA) extracts latent features by minimizing the variation between successive samples [10]. Puli et al. [11] proposed the complex probabilistic SFA that extracts slow oscillatory features for soft sensing and fault detection. Yu et al. [12] developed an adaptive monitoring scheme based on recursive exponential SFA for fine-scale adaptive processes monitoring. By linking the extracted features with classifiers such as support vector machine (SVM) [13] and random forest (RF) [14], the process states or the fault categories can be further identified. However, these methods have a data-dependent assumption that requires the samples of target states to be covered during training [15]. In real industrial settings, this assumption hardly holds due to safety requirements and high costs, that is, no training data are available for some specific states. For example, in gas–liquid two-phase flow, 1) Case #1: zero sample for transition states, as the flow states are typically formed by fixing flow rate of each single phase at the inlet when collecting data. 2) Case #2: zero sample for dangerous flow states, since they are not allowed to form in practical industries due to their destructive nature, such as slug flow [16]. 3) Case #3: zero sample for offset flow conditions, since there may be a large deviation between the actual and premodeled flow conditions for the same flow states in industrial two-phase flow.

Manuscript received 5 June 2023; revised 14 November 2023; accepted 5 February 2024. Date of publication 8 March 2024; date of current version 5 June 2024. This work was supported in part by the National Natural Science Foundation of China under Grant 51976137 and Grant 62373277. Paper no. TII-23-2024. *(Corresponding author: Shumei Zhang.)*

Linghan Li, Xinyi Han, and Shumei Zhang are with the Tianjin Key Laboratory of Process Measurement and Control, School of Electrical and Information Engineering, Tianjin University, Tianjin 300072, China (e-mail: lilinghan@tju.edu.cn; hanxinyi@tju.edu.cn; shumeizhang@tju.edu.cn).

Feng Dong is with the Tianjin Key Laboratory of Process Measurement and Control, School of Electrical and Information Engineering, Tianjin University, Tianjin 300072, China, and also with the School of Information and Intelligent Engineering, Tianjin Renai College, Tianjin 301636, China (e-mail: fdong@tju.edu.cn).

Color versions of one or more figures in this article are available at https://doi.org/10.1109/TII.2024.3367045.

Digital Object Identifier 10.1109/TII.2024.3367045

In the scenarios, where no training samples are available for some specific states of gas–liquid two-phase flow, flow state identification poses a zero-shot learning (ZSL) task. ZSL is a machine learning paradigm that aims to recognize novel classes not observed during training [17]. It leverages the semantic relationship between seen and unseen classes for identification, which is described by indirect information such as attributes, text descriptions, or word embeddings. In the research works of gas–liquid two-phase flow, the intuitionistic recognition of flow state often comes from experimental research, human observation, and subjective judgment. Hence, it is rational to utilize semantic attributes characterized by human intelligence to minutely describe gas–liquid two-phase flow states. In particular, state attributes containing structure, fluctuation, and distribution are effective in describing unknown flow states and transition states. Different flow states can share the same state attributes, as many flow states have a bubble flow structure, some flow states have intermittent characteristics, and transition states possess similar characteristics of the two states before and after it. The shareability of state attributes provides the basis for attribute transfer in the common attribute space. Therefore, it is feasible to identify "unknown" flow states by composing the state attributes.

In the field of ZSL, one research direction is novel embedding methods that can better capture the semantic relationship between seen and unseen classes. For instance, Akata et al. [18] proposed a structured prediction approach to learn a joint embedding space that can encode both visual and semantic information. Another promising direction is the incorporation of auxiliary information, such as textual descriptions or cross-modal data, to improve the generalization ability of the model. For instance, Mercea et al. [19] developed a cross-modal attention mechanism to align visual and textual information for improved ZSL performance. More recently, ZSL has also been applied to some extent in industrial fields. Feng et al. [20] proposed the ZSL method for fault diagnosis of industrial processes, in which faults are described by semantic attributes and the attribute-related features are extracted by supervised principle component analysis (SPCA). However, the SPCA algorithm may not be effective in extracting features in nonlinear and dynamic processes. Gao et al. [21] proposed a ZSL method based on contractive stacked autoencoders for fault diagnosis under unknown working loads. Nonetheless, the fault categories of the training data and test data are the same, except for the fact that the data are under different workloads.

To conduct zero-shot state identification of two-phase flow, a key challenge is to construct a mapping between data and state attributes by extracting features to learn attribute knowledge. As a highly matched method for ZSL, deep learning can adaptively extract features and learn nonlinearity [22], [23]. By combining the advantages of neural networks and SFA, deep SFA is proposed to extract nonlinear dynamic features in [24]. Chiplunkar et al. [25] proposed a supervised deep SFA based on Siamese network (SSFASN) for soft sensing. However, the SSFASN constructs the regression relationship between the input and the measured data under the supervision of the true data, which may cause overfitting in the ZSL task. Besides, the one-step time dependency modeled by SFA is insufficient to reveal the information of a complex dynamic process. A recent work [26] considers the higher-order dynamics among multiple adjacent samples, which demonstrates that long-term temporal coherence from videos is effective for clustering and action recognition, and slow and steady feature analysis (S ^{2} FA) can be integrated with deep learning to improve performance. Accordingly, in this study, we extract nonlinear higher-order dynamic features under supervision in the framework of an expanded Siamese network, with 1D-convolutional neural networks (1D-CNN) as the feature extractor.

In this work, a novel zero-shot flow state identification strategy for industrial gas–liquid two-phase flow is proposed. The attributes describing the two-phase flow states are artificially designed, including attributes of structure, fluctuation, and distribution. In the strategy, the training data of known flow states are first analyzed by the proposed supervised deep slow and steady feature analysis (SD-S^2 FA) based on Siamese networks to extract attribute-relevant features under the supervision of attribute knowledge. Next, the attribute predictors from the features to attributes are constructed by SVM, RF, and naive Bayes classifier (NBC), which can transfer the attribute knowledge from training states to target states. The best attribute prediction result of the three machine learning algorithms is reserved. Finally, the flow states of the test samples can be identified by measuring the similarity between the predicted attribute vectors and attribute labels. The novelties and contributions of this study are summarized as follows.

1) It is the first time that zero-shot state identification strategy is proposed for gas–liquid two-phase flow processes, which is conducted through the semantic descriptions of different flow states, attribute mapping, and attribute transfer.
2) To create the mapping from process data to state attributes, SD-S^2 FA extracts nonlinear high-order dynamic features in an attribute-supervised manner under an expanded Siamese network architecture, in which the 1D-CNN feature extractor can capture nonlinear spatial-temporal information.

The rest of this article is organized as follows. In Section II, a brief overview of SFA and Siamese network is provided. Section III elaborates on the methodology of the proposed SD-S^2 FA based zero-shot flow state identification strategy. In Section IV, the dynamic experiment and state identification results are presented. Finally, Section V concludes this article.

II. Preliminaries

A. SFA

SFA is an emerging machine learning algorithm that extracts slowly varying features from time series data. For a data matrix $\mathbf{x}(t) = [\mathbf{x}_1(t), \mathbf{x}_2(t), \ldots, \mathbf{x}_J(t)]^T$, the linear transformation of SFA is defined as $\mathbf{s}_j(t) = g_j(\mathbf{x}(t))$. SFA extracts features $\mathbf{s}(t) =$

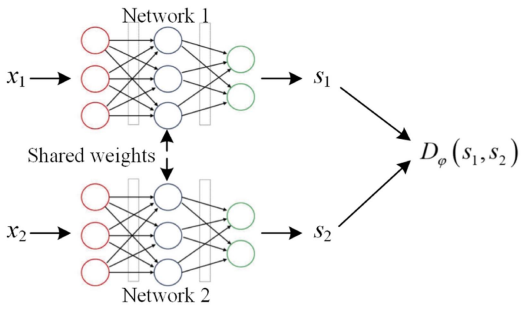

Fig. 1. Schematic diagram of Siamese network.

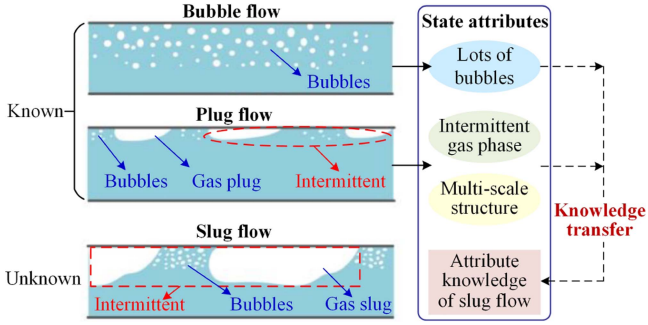

Fig. 2. Attribute knowledge transfer from known to unknown flow states.

$[\mathbf{s}_1(t), \mathbf{s}_2(t), \ldots, \mathbf{s}_J(t)]^T$ with minimal slowness $\Delta(\mathbf{s}_j)$

$$\min_{g_j(\cdot)} \Delta(\mathbf{s}_j) \triangleq \left\langle \dot{\mathbf{s}}_j^2 \right\rangle_t$$

$$s.t. \begin{cases} \langle \mathbf{s}_j \rangle_t = 0 & \text{(zero mean)} \\ \left\langle \mathbf{s}_j^2 \right\rangle_t = 1 & \text{(unit variance)} \\ \forall i \neq j : \langle \mathbf{s}_i \mathbf{s}_j \rangle_t = 0 & \text{(decorrelation)} \end{cases} \tag{1}$$

where $\dot{s}(t) \approx s(t) - s(t-1)$ denotes the time derivative, $\langle \mathbf{s} \rangle_t$ is the time averaging of $\mathbf{s}$, and $\left\langle \dot{\mathbf{s}}_j^2 \right\rangle_t$ refers to the slowness.

In SFA, each slow feature $\mathbf{s}_j(t)$ is a linear combination of all the input signals

$$\mathbf{s}_j(t) = \mathbf{w}_j^T \mathbf{x}(t). \tag{2}$$

The coefficient matrix $\mathbf{W}$ can be obtained by solving the generalized eigenvalue problem

$$\mathbf{AW} = \mathbf{BW\Omega} \tag{3}$$

where $\mathbf{W} = [\mathbf{w}_1, \mathbf{w}_2, \ldots, \mathbf{w}_J]^T$; $\mathbf{\Omega} = \text{diag}\{\omega_1, \omega_2, \ldots, \omega_J\}$ is a diagonal matrix with eigenvalues $\omega_j = \left\langle \dot{\mathbf{s}}_j^2 \right\rangle_t$; $\mathbf{A} = \left\langle \dot{\mathbf{x}} \dot{\mathbf{x}}^T \right\rangle_t$ and $\mathbf{B} = \left\langle \mathbf{x}\mathbf{x}^T \right\rangle_t$.

Finally, slow features $\mathbf{s}$ can be extracted as

$$\mathbf{s} = \mathbf{W}\mathbf{x}. \tag{4}$$

B. Siamese Network

The Siamese network is composed of two neural networks that share the same structure and weights [27]. The diagram of the Siamese network is presented in Fig. 1. The two subnetworks map the two inputs, x_1 and x_2, to new spaces to extract features individually. By calculating the loss function, the similarity of the two features is evaluated and optimized. The output of the Siamese network is a difference metric between the two features, shown as follows:

$$D_\varphi(s_1, s_2) = \|s_1 - s_2\| \tag{5}$$

where $s = \varphi(x)$ is the latent feature extracted by the neural network.

Then, the loss function is given as

$$L(\varphi, Y, x_1, x_2) = \frac{1}{2}(1-Y)(D_\varphi(s_1, s_2))^2 + \frac{1}{2} Y \{\max(0, m - D_\varphi(s_1, s_2))\}^2 \tag{6}$$

where $Y = 0$ if x_1 and x_2 are deemed similar, and $Y = 1$ if they are deemed dissimilar; $m > 0$ is a margin that defines a radius around s.

Dissimilar pairs only contribute to the loss function if their distance falls within a certain radius. It is apparent that when two input samples are similar, a smaller distance between their features will result in a smaller loss. Conversely, when two samples are dissimilar, a larger distance between the features will generate a smaller loss.

III. Methodology

A. Problem Statement and Motivation

For gas–liquid two-phase processes with varying flow conditions and complex flow natures, the difficulty of data acquisition and nonlinear dynamics of processes bring considerable challenges for flow state identification. Here, they are presented to explain the motivations for this study.

Statement 1: Although collecting training data for some specific flow states can be difficult, the attribute knowledge of them can be learned from the known states, since they may possess similar properties and structures.

As presented in Fig. 2, the definition of bubble flow is "the continuous water phase is mixed with a large number of small dispersed bubbles, which generally collect in the upper part of the pipe." From this, the state attributes of bubble flow can be designed, such as "*lots of bubbles*", "*dispersed gas and continuous liquid*", etc. Similarly, the definition of plug flow is "the gas flow rate increases on the basis of bubble flow, and some bubbles gather into long bubbles to form alternating gas plugs, the continuous liquid phase carries gas plugs and small bubbles along the top of the pipe." Its state attributes can be readily obtained, such as "*a few bubbles*", "*discontinuous gas and continuous liquid (intermittent)*", "*multiscale structure*", etc. Suppose that there is no training data for slug flow, but its description is known: "an intermittent flow state in which the gas slugs and liquid slugs flow alternatively, and the liquid slugs lead to the bursting and polymerization of bubbles." It can be learned that slug flow shares some similar properties with bubble flow and plug flow, which provides an approach to transfer attribute knowledge from known states to unknown states.

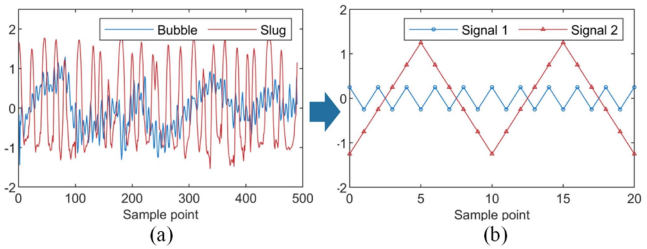

Fig. 3. Sensor signals from which "SFA" may fail to extract effective attribute-relevant features. (a) original signals. (b) abstracted signals.

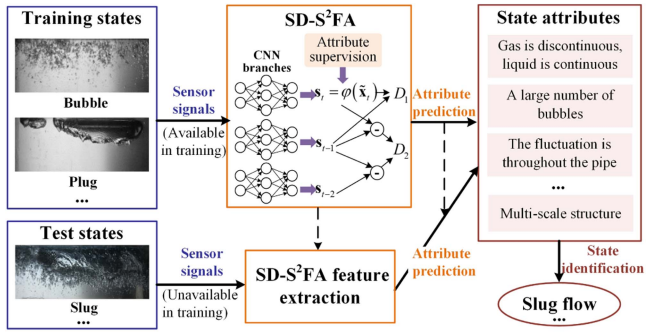

Fig. 4. Schematic diagram of zero-shot state identification strategy for gas-liquid two-phase flow.

Statement 2: A crucial aspect of zero-shot flow state identification is the feature embedding that bridges the mapping from process data to state attributes. The two-phase flow process data is highly nonlinear and dynamic, which requires effective feature extraction and information mining.

SFA is an effective method for capturing invariant and slowly varying features from input signals. Fig. 3 presents the normalized conductance signals of bubble flow and slug flow. Within one wave cycle of the slug flow, the signal of the bubble flow fluctuates for several cycles, which can be abstracted as signals in Fig. 3(b) in ideal situation. The slowness of signal 1 and 2 are the same when the first derivative of time is approximated by the temporal difference, whereas the first derivative of signal 1 has opposite signs and presents jitters. Obviously, the tendencies and physical meanings of the two signals are different. However, SFA cannot extract effective attribute-relevant features by the dynamic indicator of slowness, which limits its learning ability for attribute knowledge. Crucially, the first-order slowness fails to capture how the process changes over time. To handle this problem, S ^{2} FA imposes high-order temporal constraints to reduce the semantic gap between the quickly varying input signals and the slowly varying state categories.

Considering the above statements, the common state attributes are designed as intermediate level representations in ZSL to enable state identification with limited data. To address the nonlinearity and dynamic nature of the two-phase flow process, S ^{2} FA is integrated into an expanded Siamese network, referred to as SD-S^2 FA. Since the dynamic analysis method often lacks structural meaning and hardly extract spatial information among variables, the proposed SD-S^2 FA contains three identical 1D-CNNs. The schematic diagram of zero-shot flow state identification strategy is shown in Fig. 4.

B. Proposed SD-S^2 FA for Feature Extraction

In S ^{2} FA, except for the small differences between pairs of points, the consistent feature transition across triplets, i.e., the second-order steadiness, is also encouraged to extract rich dynamic information. To this end, the deep S ^{2} FA contains an expanded Siamese network consisting of three identical networks. Furthermore, it is worth noting that the dynamic features are not only related to the sampling point at the current moment, but also to the previous time series. Therefore, the process data should first be temporally extended by p steps to form a data frame

$$\tilde{\mathbf{x}}_t = [\mathbf{x}_t, \mathbf{x}_{t-1}, \ldots, \mathbf{x}_{t-p+1}]^T \in \Re^{p\times J} \tag{7}$$

where J is the dimension of process variables, and the time lag p is determined by the autocorrelation analysis [28].

Then, the unsupervised objective function is given as

$$\begin{aligned} L(\varphi, \tilde{\mathbf{x}}_t) &= D_\varphi(\mathbf{s}_t, \mathbf{s}_{t-1}) + \lambda D_\varphi(\mathbf{s}_t - \mathbf{s}_{t-1}, \mathbf{s}_{t-1} - \mathbf{s}_{t-2}) \\ &\quad + \eta \|\mathrm{cov}(\mathbf{s}) - \mathbf{I}\|_F \end{aligned} \tag{8}$$

where $\mathbf{s}_t = \varphi(\tilde{\mathbf{x}}_t)$ is the extracted feature at time t; D_φ is set as the Euclidean distance in this work, i.e., $D_\phi(\mathbf{s}_1, \mathbf{s}_2) = \|\mathbf{s}_1 - \mathbf{s}_2\|_2$; λ controls the relative impact of the slowness and steadiness; $\eta\|\mathrm{cov}(\mathbf{s}) - \mathbf{I}\|_F$ is the constraint of decorrelation and unit variance, $\|\cdot\|_F$ is the Frobenius norm. For sequential triplets in a temporal neighborhood, $L(\varphi, \tilde{\mathbf{x}}_t)$ penalizes distance between the adjacent pairwise feature difference vectors. In this way, combining the first-order and high-order temporal coherence among the data frames with the temporal correlation between sampling points, the complex dynamics at multiple scales can be effectively extracted.

To achieve attribute transfer for cross-class learning and avoid overfitting, the features are required to be attribute-relevant rather than data-relevant or class-relevant. Hence, the loss function of SD-S^2 FA for zero-shot flow state identification is formulized as

$$\begin{aligned} L(\varphi, \tilde{\mathbf{x}}_t) &= D_\varphi(\mathbf{s}_t, \mathbf{s}_{t-1}) + \lambda D_\varphi(\mathbf{s}_t - \mathbf{s}_{t-1}, \mathbf{s}_{t-1} - \mathbf{s}_{t-2}) \\ &\quad + \eta \|\mathrm{cov}(\mathbf{s}) - \mathbf{I}\|_F + \mu \|\boldsymbol{a}_t - \hat{\boldsymbol{a}}_t\|_2 \end{aligned} \tag{9}$$

$$\hat{\boldsymbol{a}}_t = g(\mathbf{s}_t) = \arg\max_{\boldsymbol{a}} p(\boldsymbol{a}|\mathbf{s}_t) \tag{10}$$

where $\hat{\boldsymbol{a}}_t$ is the predicted attribute vector; $\boldsymbol{a}_t$ is the true attribute vector; $\mu\|\boldsymbol{a}_t - \hat{\boldsymbol{a}}_t\|_2$ minimizes the error between them, which is weighted by the hyperparameter μ.

In this work, the hidden layer of each sub-network is composed of 1D convolution layer and pooling layer, which have been widely used for encoding input signals into latent features and extracting spatial-temporal correlation between variables and samples [29]. The convolutional kernel is defined as $\omega \in \Re^{p\times q}$. During training, 1D-CNN slides the receptive field r steps at a time in the direction of variable. The convolution operation

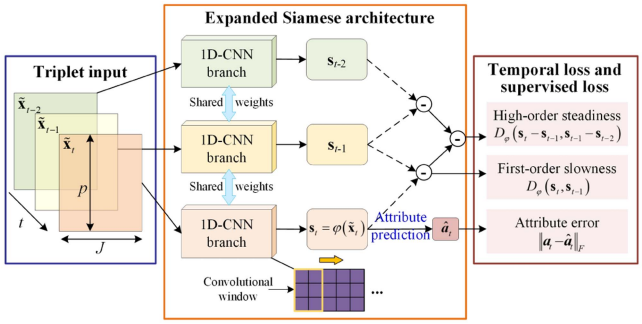

Fig. 5. Schematic diagram of 1D-CNN based SD-S^2 FA.

of 1D-CNN is formalized as

$$h_i = \sigma\left(\sum_{k=1}^{p}\sum_{l=1}^{q}\omega_{k,l} \times x_{k+i\times r,l}\right), 0 \le i \le (J-q)/r+1. \tag{11}$$

The rectified linear unit activation function $\sigma(\cdot)$ is utilized to nonlinearize the neural network to improve the feature extraction ability. Following that, the output dimension is reduced by the maximum pooling layer. By stacking the convolution layer and pooling layer, the receptive field can be expanded. Notably, the structures and parameters of the subnetworks are the same in the expanded Siamese network. The schematic of SD-S^2 FA is shown in Fig. 5.

The attribute predictor is preliminarily trained with the feature extractor under the same framework, which is learned by SVM, RF, and NBC. The best result of the three methods will be chosen as the final attribute prediction result.

C. Zero-Shot Flow State Identification Strategy

The zero-shot state identification problem of industrial gas–liquid two-phase flow is formulated as follows. In this task, two disjoint sets of classes are given: K known classes in Y and U unknown classes in Z, and $Y \cap Z = \emptyset$. Suppose that $\{(x_1, y_1), \ldots (x_N, y_N)\} \subset X \times Y$ are the labeled training samples, where $x_i \in X$ is an arbitrary instance and $y_i \in Y$ is the category label. The task is learning the classifier $f : X \to Z$ that identifies the unknown flow states. To identify the flow states for which no training data is available, the coupling class-level state attribute matrix $\boldsymbol{A} = \{\boldsymbol{a}_1, \ldots, \boldsymbol{a}_K, \boldsymbol{a}_{K+1}, \ldots, \boldsymbol{a}_{K+U}\}$ are designed artificially. Then, zero-shot flow state identification strategy can be formulized mathematically by a mapping H from X to Z

$$H = P\left(F(X)\right), F : X \to \boldsymbol{A}, P : \boldsymbol{A} \to Z. \tag{12}$$

For uniform and accurate expression, the zero-shot flow state identification strategy is presented in the form of probability. The specific implementation steps are as follows.

Step 1: For a typical gas–liquid flow state, each attribute a_m is represented by a binary value, indicating whether the flow state has the attribute. For a transition state, the attribute is obtained by the weighted sum of the attribute values of two typical states before and after it, representing the degree or probability of an attribute. And thus, any flow state (including seen and unseen states) can be described and labeled by a fixed-length binary vector $\boldsymbol{a} = (a_1, \ldots, a_M)$, which can be shared by the training classes and test classes.

Step 2: All the training samples are used to learn the feature extractor by the proposed SD-S^2 FA under the supervision of attributes, as introduced in Section III-B. It is worth noting that the preliminary attribute predictor is pretrained with the feature extractor simultaneously.

Step 3: Traditional DAP learns the classifier for each attribute separately. In order to learn multiple attribute classifiers at the same time, attribute learning is regarded as a multitasking learning in this work

$$\min_{G} \|\boldsymbol{A} - \boldsymbol{G}(\mathbf{s})\|_F \tag{13}$$

where $\boldsymbol{G}(\cdot) = [g_1(\cdot), g_2(\cdot), \ldots, g_M(\cdot)]$ is the mapping set from features to state attributes. The attribute predictor $\hat{\boldsymbol{A}} = \boldsymbol{G}(\mathbf{s})$ can be established by SVM, RF or NBC. Among them, SVM operates by finding the optimal hyperplane that maximally separates different classes in a high-dimensional feature space, which is widely applied in various fields due to its ability to handle nonlinear data and its robustness against overfitting [13]. RF combines the predictions of multiple decision trees to provide accurate and reliable classification and regression results [14]. Moreover, NBC predicts the probability of a sample belonging to a specific class based on the presence of certain features [30]. All the three methods can provide the estimation $p(a_m|\mathbf{s})$ from the feature $\mathbf{s}$ to each attribute a_m.

The complete attribute prediction is achieved by combining all the attributes

$$p\left(\boldsymbol{a}|\mathbf{s}\right) = \prod_{m=1}^{M} p\left(a_m|\mathbf{s}\right). \tag{14}$$

Step 4: Since the attribute vector a^z of each test class z is known, the target flow state category can be inferred using the predicted attributes through Bayes' rule

$$p\left(z|\boldsymbol{a}\right) = \frac{p(a|z)p(z)}{p\left(\boldsymbol{a}^z\right)} = \begin{cases} \frac{p(z)}{p(\boldsymbol{a}^z)}, \boldsymbol{a} = \boldsymbol{a}^z \\ 0, \boldsymbol{a} \ne \boldsymbol{a}^z. \end{cases} \tag{15}$$

Combining the mapping from process data to state attributes, the posterior of the target category can be calculated using the test sample

$$p\left(z|\boldsymbol{x}\right) = \sum_{\boldsymbol{a}\in\boldsymbol{A}} p\left(z|\boldsymbol{a}\right) p\left(\boldsymbol{a}|\mathbf{s}\right) = \frac{p(z)}{p\left(\boldsymbol{a}^z\right)} \prod_{m=1}^{M} p\left(a_m^z|\varphi(\boldsymbol{x})\right). \tag{16}$$

Step 5: The output class is assigned as the state category with the largest posterior probability

$$f\left(\boldsymbol{x}\right) = \arg\max_{j=1,\ldots,U} p\left(z|\boldsymbol{x}\right). \tag{17}$$

IV. Experiments and Results

A. Dynamic Experiment of Gas–Liquid Two-Phase Flow

The dynamic experiment of gas–liquid two-phase flow is conducted on the multiphase flow experimental facility, as presented in Fig. 6. The gas phase is dry air (density 1.2 kg/m^3, dynamic viscosity 1.81×10^{-5}Pa · s), and the liquid phase is tap water (density 998 kg/m^3, dynamic viscosity 1.01×10^{-3}Pa · s). The

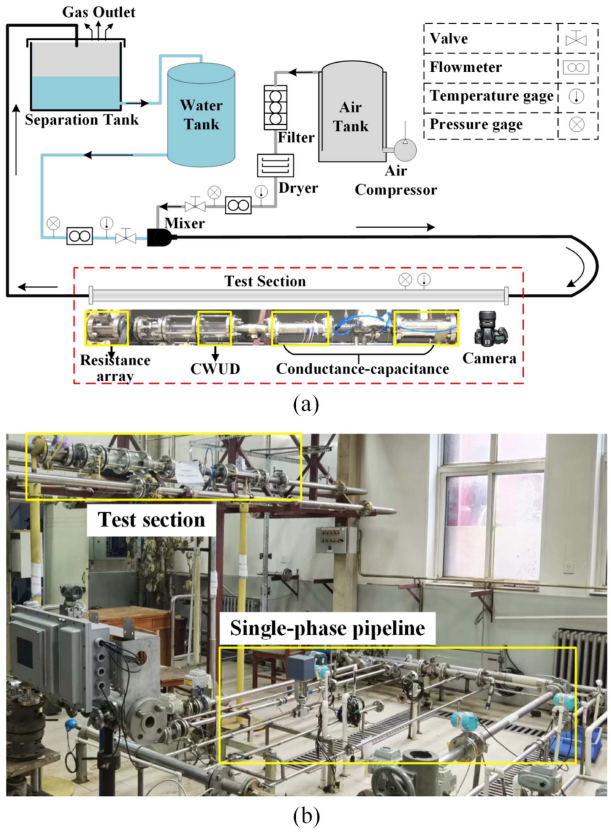

Fig. 6. Multiphase flow facility. (a) schematic, (b) actual devices.

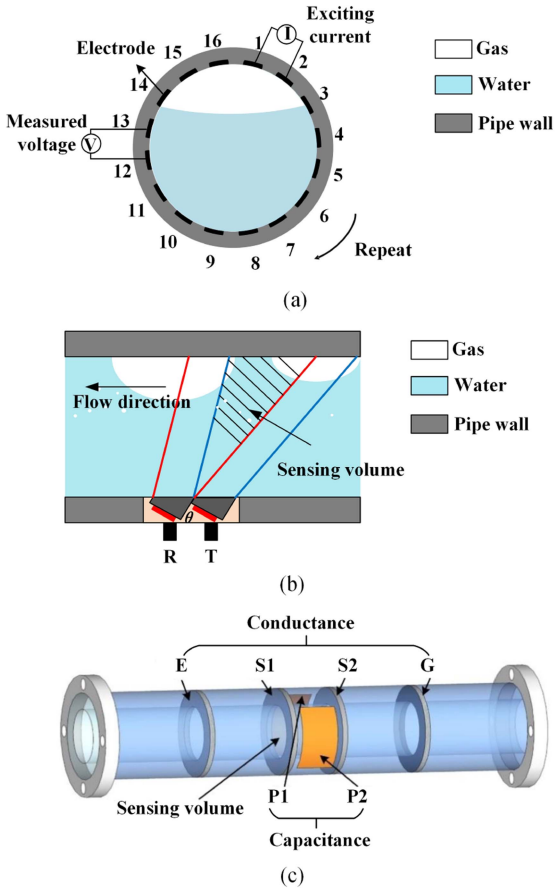

Fig. 7. Structure and measurement principle of sensors. (a) resistance array, (b) CWUD, (c) capacitance–conductance.

pipe is made of stainless steel with an inner diameter of 50 mm, and the total length of horizontal pipe is 16.6 m. The flow rate of each phase is controlled by the pump and valve of the single-phase pipeline. The test section is located 13 m downstream from the inlet to ensure the flow state to fully develop. Due to the difficulty of zero-shot state identification and the requirement for all-sided attribute mapping, multiple sensors are installed at the test section, including the resistance array [31], continuous wave ultrasonic Doppler (CWUD) sensor [4] and capacitance–conductance sensor [2]. Moreover, a high-speed camera is used to record the flow state. The high dimensional data can fully reflect the information of the two-phase flow state, which are used for the training and test of zero-shot flow state identification. The structure and measurement principle of multiple sensors in the test section are illustrated in Fig. 7. The introduction and data processing procedures for these sensors are outlined as follows.

The resistance array comprises 16 electrodes, providing information of medium distribution, as shown in Fig. 7(a). The current is injected into adjacent pairs of electrodes and the voltages are measured from successive neighboring electrode pairs. This process is iteratively repeated. The mean characteristic, denoted as V_{Ri}, is computed from the boundary voltages in the ith excitation cycle

$$V_{Ri} = \frac{1}{13}\sum_{j=1}^{13}(V_{ij} - V_{ij0}) \tag{18}$$

where V_{ij} is the jth boundary voltage measured in the ith excitation. V_{ij0} denotes the boundary voltage in the condition that the pipe is filled with water.

The CWUD can provide information of flow velocity, as presented in Fig. 7(b). According to the Doppler effect, the ultrasonic data is processed to obtain Doppler velocity u_{dop}

$$u_{\mathrm{dop}} = \frac{c\bar{f}_d}{2f_0\cos\theta} \tag{19}$$

where f_0 is the frequency of the ultrasound emission signal, θ is the Doppler angle, $\bar{f}_d$ is the average Doppler shift, and c is the sound speed in water.

The capacitance–conductance sensor can capture information of the phase holdup, as depicted in Fig. 7(c). The conductance consists of four ring electrodes (E, S1, S2, and G). An electric current is introduced into the fluid through E and G to establish an electrical sensing field between S1 and S2. The standardization of conductance signal V_{con} can be obtained by measuring the voltage between S1 and S2

$$V_{\mathrm{con}} = V_{w1}/V_{\mathrm{meas1}} \tag{20}$$

where V_{w1} is the voltage when the pipe is filled with water, V_{meas1} is the measured voltage.

For the capacitance mode, a sensing field is created between P1 and P2 by injecting an alternating voltage into fluid. The data

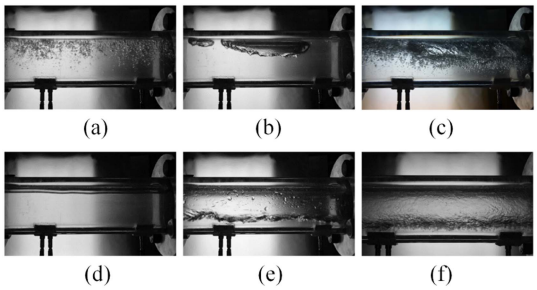

Fig. 8. Typical gas–liquid two-phase flow states. (a) bubble flow, (b) plug flow, (c) slug flow, (d) wave flow, (e) stratified flow, and (f) annular flow.

TABLE I
FLOW STATES AND EXPERIMENT CONDITIONS

No.	Flow state	Water flowrate (m^3/h)	Gas flowrate (m^3/h)
1-1	Bubble #1	10.0	1.3-2.3
1-2	Bubble #2	15.0	1.3-2.3
2-1	Plug #1	2.0	1.3-2.3
2-2	Plug #2	5.0	1.3-2.3
3-1	Slug #1	10.0	18.0-40.0
3-2	Slug #2	15.0	18.0-40.0
4-1	Wave #1	0.3	35.4-81.7
4-2	Wave #2	0.8	35.4-81.7
5-1	Stratified #1	0.3	0.7-1.6
5-2	Stratified #2	0.8	0.7-1.6
6-1	Annular #1	0.3	140.0-189.3
6-2	Annular #2	0.8	140.0-189.3
7	Transition from bubble to slug	10.0, 15.0	6.9
8	Transition from plug to slug	2.0, 5.0	18.6
9	Transition from slug to annular	10.0, 15.0	78.4
10	Transition from stratified to wave	0.3, 0.8	20.0

of capacitance signal is processed by the normalized relative capacitance difference V_{cap}, which reflects phase holdup when the continuous phase is nonconductive

$$V_{\text{cap}} = (V_{\text{meas2}} - V_o)/(V_{w2} - V_o) \tag{21}$$

where V_{w2} is the voltage when the pipe is filled with water, V_o is the voltage when the pipe is filled with nonconductive phase, V_{meas2} denotes the measured voltage.

In gas–liquid two-phase flow experiment, the collected dataset comprises six typical flow states, namely bubble flow, plug flow, slug flow, wave flow, stratified flow, and annular flow. Their photos are presented in Fig. 8. Besides, the dataset contains four transition states, including bubble flow to slug flow, plug flow to slug flow, slug flow to annular flow, and stratified flow to wave flow. Moreover, for each typical flow state, the single flow rates are set differently to simulate the offset flow conditions. Each flow state is described by 12 variables, and trained with 2000 samples. The flow states and corresponding flow conditions are listed in Table I.

TABLE II
ATTRIBUTE DEFINITION FOR GAS–LIQUID TWO-PHASE FLOW

No.	State attributes
1	The gas phase and liquid phase are continuous
2	The gas is discontinuous, the liquid is continuous
3	The gas is dispersed, the liquid is continuous
4	The liquid phase is always in contact with the upper and lower parts of the pipe
5	An open interface exists between the two phases
6	A large number of bubbles exist
7	A small number of bubbles exist
8	The droplets exist
9	The fluctuation is distributed throughout the pipe
10	The fluctuation is concentrated in the upper part of the pipe
11	The fluctuation is concentrated in the lower part of the pipe
12	Multiscale structure
13	The fluctuation is slight

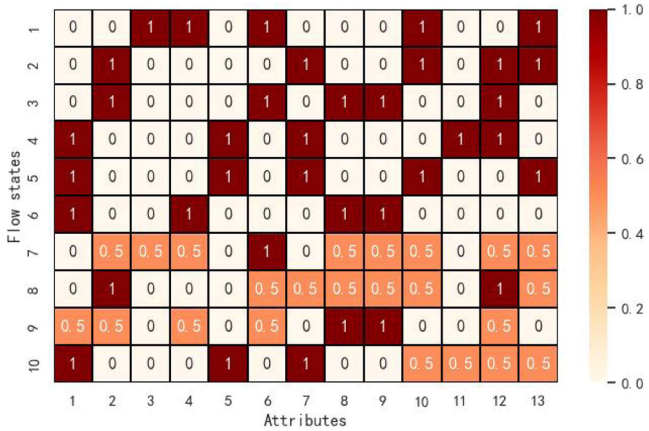

Fig. 9. Class-attribute matrix of gas–liquid two-phase flow.

TABLE III
FOUR CASE SETTINGS FOR ZERO-SHOT FLOW STATE IDENTIFICTAION

Case.	Training states	Testing states
1	1~6	7~10
2-1	1, 2, 5, 6	3, 4
2-2	1, 2, 4, 5	3, 6
3	1-1, 2-1, 3-1, 4-1, 5-1, 6-1	1-2, 2-2, 3-2, 4-2, 5-2, 6-2

B. Results and Discussions

In this work, according to a wealth of experimental observations and existing foundational research works on gas–liquid two-phase flow [4], [32], [33], [34], 13 fine-grained state attributes are defined for describing different flow states of gas–liquid two-phase flow, as presented in Table II. The designed attributes are associated with flow continuity, flow structure, and distribution of fluctuations. Correspondingly, the class-attribute matrix $\boldsymbol{A}$ is presented in Fig. 9, where "1" indicates the presence of a particular attribute, "0" denotes the absence of the attribute, and "0.5" represents the degree or probability of transition state attributes. Besides, to simulate scenarios involving a lack of samples in industrial gas–liquid two-phase flow, four distinct cases are designed as in Table III. These cases include zero

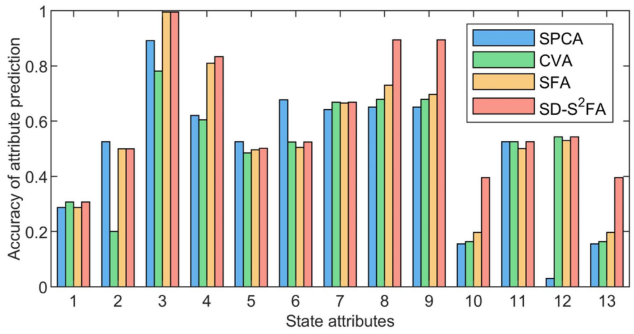

Fig. 10. Accuracy of attribute prediction for Case #2-1.

sample case for transition states, zero sample cases for dangerous flow states, and zero sample case for flow states with offset flow conditions. It is crucial to emphasize that data pertaining to the target states have been intentionally excluded from the training dataset, and they are solely employed as test data for evaluating the model's performance.

1) Contrast Experiment: The SD-S^2 FA based zero-shot flow state identification strategy is applied to the gas–liquid two-phase flow process to illustrate its efficacy and superiority. In this work, the attribute-relevant features are extracted by the proposed SD-S^2 FA, and its performance is compared with traditional SFA [10], canonical variate analysis (CVA) [35], and SPCA [20]. Afterward, the SVM, RF, and NBC are all conducted to learn the attribute predictor, and the best result for attribute prediction of the three machine learning algorithms is reserved. The kernel function of SVM is set as RBF kernel, and the number of decision trees of RF is set as 100. Finally, the similarity between the predicted attributes of the test sample and the attribute labels of the flow state categories are measured using Euclidean distance to identify the target state.

Effective feature extraction and attribute learning are crucial for the performance of zero-shot flow state identification. For example, in Case #2-1, state features are extracted by the four feature extraction methods, and then the attributes are predicted. The accuracy of attribute prediction for Case #2-1 is shown in Fig. 10. It is observed that the prediction accuracies of SD-S^2 FA for fluctuation-relevant attributes are significantly higher than other methods, especially for attributes 3, 4, 8, 9, and 13. Due to the coexistence of the first order and high order temporal coherence, SD-S^2 FA can characterize fluctuations at different scales with different variation trends. It further facilitates that the proposed method effectively capture the complex dynamics of two-phase flow processes. Furthermore, in predicting other attributes, this method demonstrates performance levels that are comparable to those achieved by the other methods.

The confusion matrices of the zero-shot flow state identification methods based on SD-S^2 FA, traditional SFA, CVA, and SPCA for Case #1 are presented in Fig. 11. The vertical coordinate represents the real category of test samples, and the horizontal coordinate represents the category predicted by the models. The evolving dynamic mechanism of transition states highlights the importance of nonlinear higher-order temporal correlation in attribute prediction. Thus, the proposed SD-S^2 FA

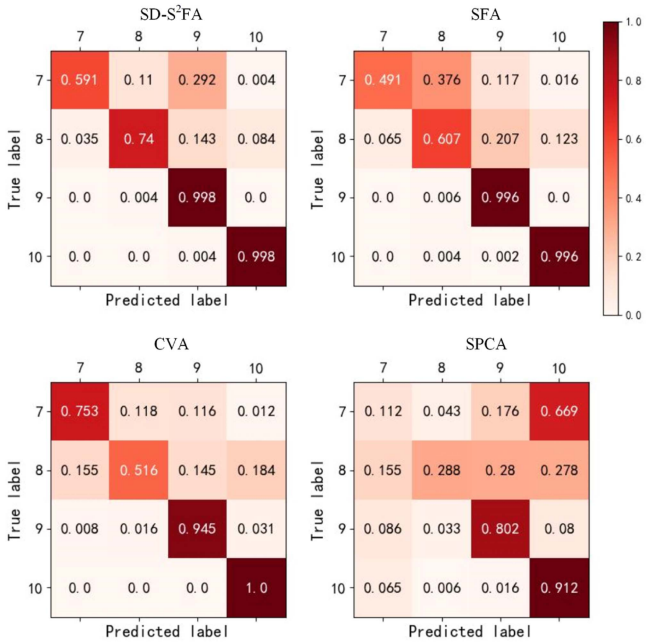

Fig. 11. Confusion matrices between four test classes of the transition states (Case #1) using the four methods.

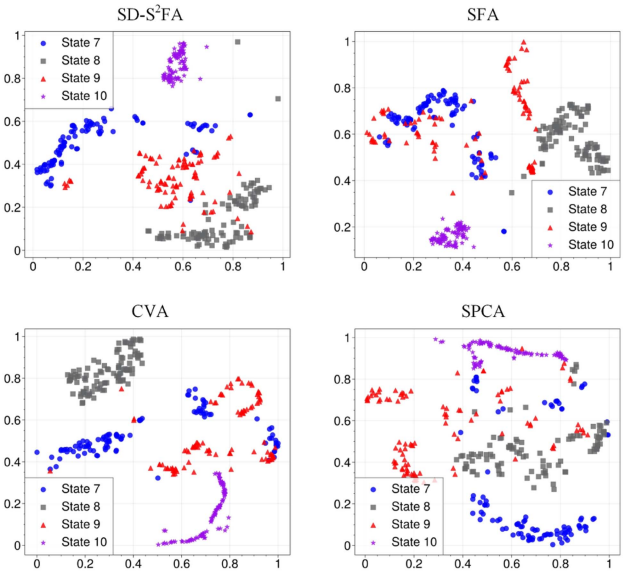

Fig. 12. T-SNE visualization of the features extracted by the four methods for Case #1.

outperforms the other methods with the highest classification accuracy of 83.18%, which is significantly better than random guessing (25% accuracy). The SFA and CVA methods also yield commendable results, attaining accuracy rates of 77.09% and 80.36%, respectively. These two methods take into account dynamic and serial correlation, which are crucial for characterizing transition states, as the state at a previous moment significantly influences the state at a subsequent moment during transitions. In contrast, the identification accuracy is only 52.86% when using SPCA for feature extraction. This is because SPCA only considers the linear information of static variance of the flow

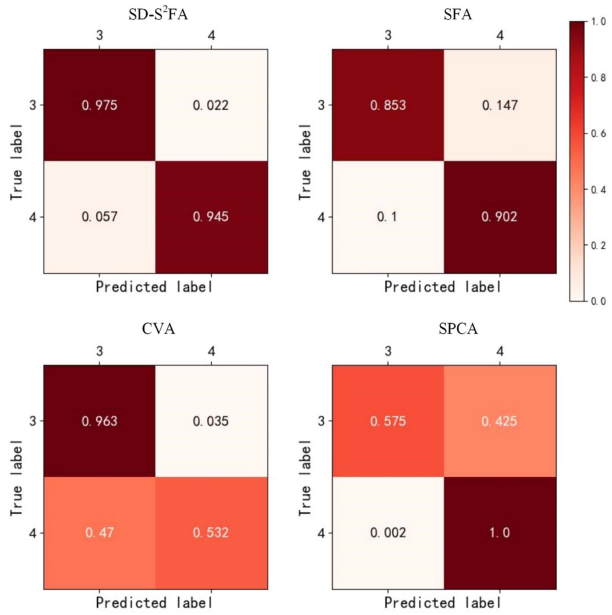

Fig. 13. Confusion matrices between two test classes of slug flow and wave flow (Case #2-1) using the four methods.

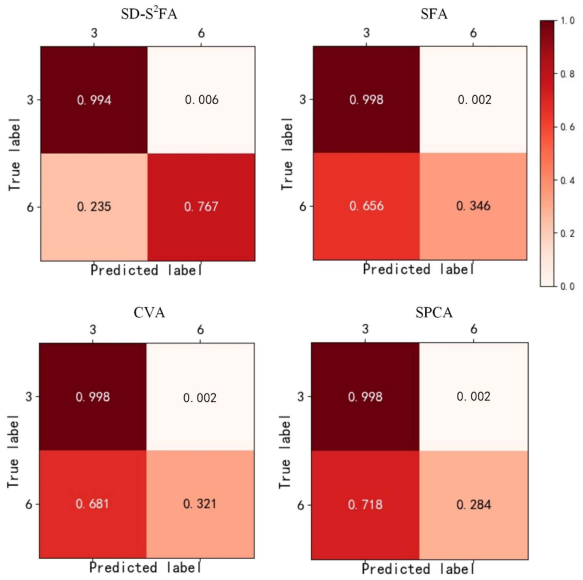

Fig. 14. Confusion matrices between two test classes of slug flow and annular flow (Case #2-2) using the four methods.

process and fails to capture the evolving dynamic mechanism of transition states.

To further assess the discriminability of different feature extraction methods, Fig. 12 shows the T-SNE [36] visualization of the features extracted by the four methods in a 2-D feature space for Case #1. It is evident that our model notably enhances the discriminability of the features, generating more distinct boundaries among feature sets. Conversely, the overlapping among different feature sets extracted by the other methods is larger, especially for State 7 and State 8.

The confusion matrices of flow state identification results for Case #2-1 and #2-2 are depicted in Figs. 13 and 14, respectively,

TABLE IV
ACCURACIES OF ZERO-SHOT FLOW STATE IDENTIFICATION BASED ON DIFFERENT FEATURE EXTRACTION METHODS

Case.	SD-S^{2}FA	SFA	CVA	SPCA
1	**83.18%**	77.09%	80.36%	52.86%
2-1	**96.01%**	86.94%	74.74%	78.57%
2-2	**88.05%**	67.20%	65.95%	64.10%
3	**79.79%**	75.91%	68.39%	65.37%

The bold values represent the highest accuracies among all methods.

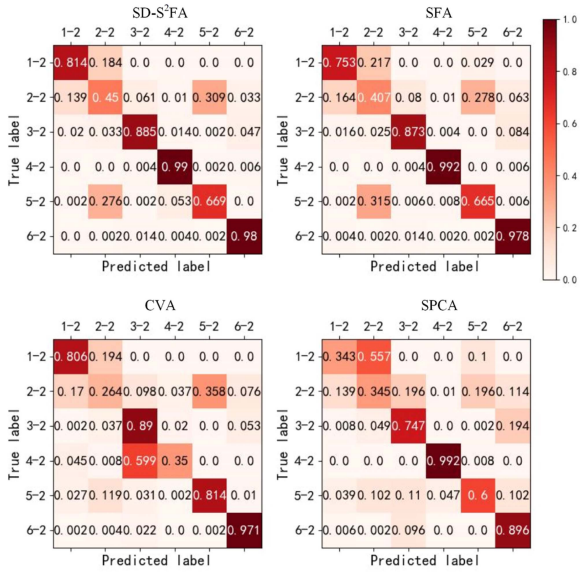

Fig. 15. Confusion matrices between six test classes of states with offset flow conditions (Case #3) using the four methods.

which focus on the scenario where no samples are available for dangerous flow states. In Fig. 13, for slug flow and wave flow without available training samples, they exhibit distinct multiscale structures and dramatic fluctuations compared to other flow states. These characteristics are primarily represented by the change speed and stability of the features. As a result, the proposed SD-S^2 FA demonstrates the highest identification accuracy of 96.01%. In addition, SFA achieves a relatively high identification accuracy of 86.94%. However, in contrast, CVA and SPCA exhibit poor performance for identifying dangerous flow states without training samples. CVA mainly extracts the global serial correlation of a process by maximizing the correlation between past and future time series, which often ignores microscale variations. On the other hand, SPCA fails to capture process dynamics, resulting in a inferior performance. In Fig. 14, the proposed method attains an identification accuracy of 88.05%, which is lower than that in Case #2-1. Besides, the accuracies of the other methods remain below 70%. It can be explained by the flow state attribute description, where only slug flow and annular flow possess attribute 8 and 9. This attribute distribution impedes knowledge transfer from the source domain to the target domain in zero-shot flow state identification, since these two attributes are not distinguishable.

In Fig. 15, the accuracies of all the state identification methods for Case #3 are significantly higher than the chance level of

TABLE V
RESULTS OF ABLATION STUDY

	Nonlinearity	Slowness	Steadiness	Supervision	Case #1 Acc	Case #2-1 Acc	Case #2-2 Acc	Case #3 Acc
SFA		✓			76.29%	81.17%	67.20%	75.91%
D-SFA	✓	✓			76.50%	77.23%	71.14%	76.82%
SD-SFA	✓	✓		✓	78.09%	87.24%	80.36%	78.91%
SD-S^2FA	✓	✓	✓	✓	**83.18%**	**92.08%**	**84.17%**	**79.79%**

The bold values represent the highest accuracies among all methods.

16.67%. This demonstrates the potential of using state attributes for state identification in the context of offset working conditions. Nevertheless, the low accuracies of certain flow state categories, such as 45% for plug flow, are primarily due to the difficulty of zero-shot state identification and the complexity of the process. There are also similar characteristics between different flow states, such as plug flow and stratified flow, which require well-designed attribute descriptions to reveal the commonality and heterogeneity between different flow states. Despite these challenges, the SD-S^2 FA method still achieves a relatively high accuracy of 79.79%, outperforming the other three methods. Finally, the accuracies of the proposed SD-S^2 FA, SFA, CVA, and SPCA for the four cases are compared in Table IV.

2) Ablation Study: To validate the effectiveness of nonlinearity processing, higher-order temporal generalization and attribute supervision, the traditional linear SFA is taken as the baseline. On this basis, the Siamese network is introduced to extract slow features under the framework of deep learning. Besides, we generalize from pairs of temporally close samples to triplets of samples. The Siamese architecture with two identical networks is generalized to an expanded Siamese architecture with three identical networks to capture both the slowness and steadiness. Moreover, to prove the necessity of attribute supervision, SD-S^2 FA is carried out in a supervised manner. Then, the attribute predictor is fixed as RF. Following that, same as the contrast experiment, the flow state is identified by comparing the Euclidean distance between state attributes.

The results of the ablation study are presented in Table V. It showcases the consecutive enhancement in identification performance achieved by the complete SD-S^2 FA model over the base SFA model. The improvements are quantified at 6.89%, 10.91%, 16.97%, and 3.88% for the four respective cases. In comparison to linear SFA, the D-SFA prompts the model to extract nonlinearity from the flow process, resulting in an average performance boost of 0.28%. The improvement effect is relatively significant in Case #2-2 and Case #3, whereas the model's performance is barely improved in the other two cases. Since RF is fixed as the attribute predictor, which is a nonlinear classifier, the nonlinear relationship of the process has been considered during state identification. Consequently, the nonlinearity processing during feature extraction has light influence on zero-shot state identification accuracy. Another reason is that the nonlinear relationship of the process may be not significant in Case #1 and Case #2-1.

Furthermore, when compared to the unsupervised D-SFA, the attribute supervision of SD-SFA assumes a pivotal role in guiding the learning of each attribute and enforcing the features to encapsulate fine-grained information. This supervision provides an average accuracy gain of 5.73%. In addition, after introducing the second-order temporal coherence (steadiness) into the Siamese network architecture, the overall zero-shot state identification rate increases by 3.66%. Especially for the identification of transition states, the accuracy increases by 5.09%. The experimental results demonstrate that the state attribute-relevant features are more powerful for learning semantic knowledge of flow states. Besides, extracting both the first-order and higher-order temporal information can effectively improve the methods' performance. Particularly, the higher-order dynamic information is crucial for characterizing transition states and dangerous states since the dynamic processes possess strong temporal correlation.

V. CONCLUSION

This article proposes the SD-S^2 FA-based strategy to address the problem of zero-shot state identification for industrial gas–liquid two-phase flow. In this method, the mapping from sample space to attribute space is realized by extracting attribute-relevant features under the supervision of attributes. To extract complex nonlinear dynamic features, the one-step temporal dependency is generalized to the first and high-order temporal constraints, which is implemented under an expanded Siamese network architecture with 1D-CNN as the feature extractor. By providing an attribute learning structure from the perspective of temporal relation and attribute relevance, the proposed approach effectively avoids overfitting and realizes attribute transfer. The two-phase flow states are described by the state attributes shared among different state categories, which allows for zero-shot state identification through attribute transfer and attribute prediction. In future work, we plan to explore generalized ZSL (GZSL) to identify both seen and unseen flow states simultaneously while improving the domain migration problem. In addition, the zero-shot state identification of oil–gas–water three-phase flow presents a challenging and meaningful area for future research.

REFERENCES

[1] D. Hu, J. Li, Y. Liu, and Y. Li, "Flow adversarial networks: Flowrate prediction for gas-liquid multiphase flows across different domains," *IEEE Trans. Neural Netw. Learn. Syst.*, vol. 31, no. 2, pp. 475–487, Feb. 2020.

[2] X. Shi, C. Tan, H. Wu, and F. Dong, "An electrical and ultrasonic doppler system for industrial multiphase flow measurement," *IEEE Trans. Instrum. Meas.*, vol. 70, Jan. 2021, Art. no. 7500313.

[3] S. Wöckel, U. Hempel, and J. Auge, "Acousto-capacitive tomography of liquid multiphase systems," *Sensors Actuators A- Phys.*, vol. 172, pp. 322–329, 2011.

[4] X. Dong, C. Tan, and F. Dong, "Gas-liquid two-phase flow velocity measurement with continuous wave ultrasonic Doppler and conductance sensor," *IEEE Trans. Instrum. Meas.*, vol. 66, no. 11, pp. 3064–3076, Nov. 2017.
[5] E. Hervieu, E. Jouet, and L. Desbat, "Development and validation of an X-ray tomograph for two-phase flow," *Ann. New York Acad. Sci.*, vol. 972, pp. 87–94, 2002.
[6] J. E. Julia, W. K. Harteveld, R. F. Mudde, and H. van den Akker, "On the accuracy of the void fraction measurements using optical probes in bubbly flows," *Rev. Sci. Instrum.*, vol. 76, 2005, Art. no. 035103.
[7] W. Wu, C. Tan, S. Zhang, and F. Dong, "Sparse local fisher discriminant analysis for gas-water two-phase flow status monitoring with multisensor signals," *IEEE Trans. Ind. Informat.*, vol. 19, no. 3, pp. 2886–2898, Mar. 2023.
[8] S. Wold, K. H. Esbensen, and P. Geladi, "Principal component analysis," *Comprehensive Chemometrics*, vol. 2, pp. 37–52, 1987.
[9] R. Muradore and P. Fiorini, "A PLS-based statistical approach for fault detection and isolation of robotic manipulators," *IEEE Trans. Ind. Electron.*, vol. 59, no. 8, pp. 3167–3175, Aug. 2012.
[10] L. Wiskott and T. J. Sejnowski, "Slow feature analysis: Unsupervised learning of invariances," *Neural Comput.*, vol. 14, pp. 715–770, 2002.
[11] V. K. Puli, R. Raveendran, and B. Huang, "Complex probabilistic slow feature extraction with applications in process data analytics," *Comput. Chem. Eng.*, vol. 154, 2021, Art. no. 107456.
[12] W. Yu and C. Zhao, "Recursive exponential slow feature analysis for fine-scale adaptive processes monitoring with comprehensive operation status identification," *IEEE Trans. Ind. Informat.*, vol. 15, no. 6, pp. 3311–3323, Jun. 2019.
[13] F. Deng, S. Guo, R. Zhou, and J. Chen, "Sensor multifault diagnosis with improved support vector machines," *IEEE Trans. Automat. Sci. Eng.*, vol. 14, no. 2, pp. 1053–1063, Apr. 2017.
[14] Z. Chai and C. Zhao, "Enhanced random forest with concurrent analysis of static and dynamic nodes for industrial fault classification," *IEEE Trans. Ind. Informat.*, vol. 16, no. 1, pp. 54–66, Jan. 2020.
[15] W. Yu, M. Wu, B. Huang, and C. Lu, "A generalized probabilistic monitoring model with both random and sequential data," *Automatica*, vol. 144, 2022, Art. no. 110468.
[16] Q. Wu, S. Zou, X. Zhang, C. Yang, T. Yao, and L. Guo, "Forecasting the transition to undesirable gas-liquid two-phase flow patterns in pipeline-riser system: A method based on fast identification of global flow patterns," *Int. J. Multiphase Flow*, vol. 149, 2022, Art. no. 103998.
[17] C. H. Lampert, H. Nickisch, and S. Harmeling, "Learning to detect unseen object classes by between-class attribute transfer," in *Proc. IEEE Conf. Comput. Vis. Pattern Recognit.*, 2009, pp. 951–958.
[18] Z. Akata, M. Malinowski, M. Fritz, and B. Schiele, "Multi-cue zero-shot learning with strong supervision," in *Proc. IEEE Conf. Comput. Vis. Pattern Recognit.*, 2016, pp. 59–68.
[19] O.-B. Mercea, L. Riesch, A. S. Koepke, and Z. Akata, "Audiovisual generalised zero-shot learning with cross-modal attention and language," in *Proc. IEEE Conf. Comput. Vis. Pattern Recognit.*, 2022, pp. 10543–10553.
[20] L. Feng and C. Zhao, "Fault description based attribute transfer for zero-sample industrial fault diagnosis," *IEEE Trans. Ind. Informat.*, vol. 17, no. 3, pp. 1852–1862, Mar. 2021.
[21] Y. Gao, L. Gao, X. Li, and Y. Zheng, "A zero-shot learning method for fault diagnosis under unknown working loads," *J. Intell. Manuf.*, vol. 31, pp. 899–909, 2020.
[22] J. Zhu, H. Bo Shi, B. Song, Y. Tao, and S. Tan, "Convolutional neural network based feature learning for large-scale quality-related process monitoring," *IEEE Trans. Ind. Informat.*, vol. 18, no. 7, pp. 4555–4565, Jul. 2022.
[23] Q. Sun and Z. Ge, "Probabilistic sequential network for deep learning of complex process data and soft sensor application," *IEEE Trans. Ind. Informat.*, vol. 15, no. 5, pp. 2700–2709, May 2019.
[24] B. Du, L. Ru, C. Wu, and L. Zhang, "Unsupervised deep slow feature analysis for change detection in multi-temporal remote sensing images," *IEEE Trans. Geosci. Remote Sens.*, vol. 57, no. 12, pp. 9976–9992, Dec. 2019.
[25] R. Chiplunkar and B. Huang, "Siamese neural network-based supervised slow feature extraction for soft sensor application," *IEEE Trans. Ind. Electron.*, vol. 68, no. 9, pp. 8953–8962, Sep. 2021.
[26] D. Jayaraman and K. Grauman, "Slow and steady feature analysis: Higher order temporal coherence in video," in *Proc. IEEE Conf. Comput. Vis. Pattern Recognit.*, 2015, pp. 3852–3861.
[27] J. Bromley et al., "Signature verification using a "siamese" time delay neural network," *Int. J. Pattern Recognit. Artif. Intell.*, vol. 7, pp. 669–688, 1993.
[28] A. Negiz and A. Çlinar, "Statistical monitoring of multivariable dynamic processes with state-space models," *Aiche J.*, vol. 43, pp. 2002–2020, 1997.
[29] W. Yu, C. Zhao, and B. Huang, "Moninet with concurrent analytics of temporal and spatial information for fault detection in industrial processes," *IEEE Trans. Cybern.*, vol. 52, no. 8, pp. 8340–8351, Aug. 2021.
[30] R. Zhen, Y. Jin, Q. Hu, Z. Shao, and N. V. Nikitakos, "Maritime anomaly detection within coastal waters based on vessel trajectory clustering and naïve Bayes classifier," *J. Navigation*, vol. 70, pp. 648–670, 2017.
[31] C. Tan, Y. Shen, K. M. Smith, F. Dong, and J. Escudero, "Gas-liquid flow pattern analysis based on graph connectivity and graph-variate dynamic connectivity of ERT," *IEEE Trans. Instrum. Meas.*, vol. 68, pp. 1590–1601, May 2019.
[32] J. M. Mandhane, G. A. Gregory, and K. Aziz, "A flow pattern map for gas-liquid flow in horizontal pipes," *Int. J. Multiphase Flow*, vol. 1, pp. 537–553, 1974.
[33] S. Agrawal, G. A. Gregory, and G. W. Govier, "An analysis of horizontal stratified two phase flow in pipes," *Can. J. Chem. Eng.*, vol. 51, pp. 280–286, 1973.
[34] D. Schubring and T. A. Shedd, "Wave behavior in horizontal annular air-water flow," *Int. J. Multiphase Flow*, vol. 34, pp. 636–646, 2008.
[35] B. Jiang, D. Huang, X. Zhu, F. Yang, and R. D. Braatz, "Canonical variate analysis-based contributions for fault identification," *J. Process Control*, vol. 26, pp. 17–25, 2015.
[36] L. van der Maaten and G. E. Hinton, "Visualizing data using t-SNE," *J. Mach. Learn. Res.*, vol. 9, pp. 2579–2605, 2008.

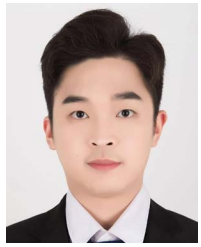

Linghan Li received the B.S. degree in automation, in 2019, from Tianjin University, Tianjin, China, where he is currently working toward the Ph.D. degree in control science and engineering.

His current research interests include multiphase flow measurement, machine learning methods, and process monitoring.

Xinyi Han received the B.S. degree, in 2023, automation from Tianjin University, Tianjin, China, where she is currently working toward the M.S. degree in control science and engineering.

Her current research interests include multiphase flow measurement, machine learning methods, and state analysis.

Feng Dong (Senior Member, IEEE) received the B.S., M.S., and Ph.D. degrees in control science and engineering from Tianjin University, Tianjin, China, in 1988, 1996, and 2002, respectively.

He is currently a Professor with the School of Electrical and Information Engineering, Tianjin University, and the School of Information and Intelligent Engineering, Tianjin Renai College. His research interests include visualization measurement and information intelligent processing of multi-phase object distribution; and on-line measuring, modeling, analyzing and diagnosing of complex process.

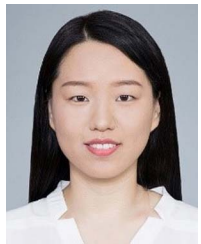

Shumei Zhang (Member, IEEE) received the B.S., M.S., and Ph.D. degrees in control science and engineering from the Department of Automation, Northeastern University, Shenyang, China, in 2009, 2011, and 2016, respectively.

She was a Postdoctoral Fellow (2016–2019) with Zhejiang University. She is currently an Associate Professor with the School of Electrical and Information Engineering, Tianjin University. Her research interests include statistical process monitoring and fault diagnosis of complex industrial processes such as batch processes and multimode processes.